ChemCatChem

Research Article
doi.org/10.1002/cctc.202400657

Chemistry Europe
European Chemical Societies Publishing

www.chemcatchem.org

Heterogeneously Catalyzed Partial Oxidation of Styrene on a Silver Surface

Rasika E. A. Dissanayake,[a, b] Arved C. Dorst,[a, b] Kerim Benfreha,[a, b] Daniel R. Killelea,[c] and Tim Schäfer*[a, b]

The epoxidation of olefins on Ag/O systems is a significant industrial-scale process within heterogeneous catalysis. However, the details of the surface reaction remain controversial, and it has been highly challenging to reconcile the findings from cataltyic studies under reaction conditions with the highly detailed static studies under carefully controlled ultra-high vacuum (UHV) conditions. In this study, we combine molecular beam surface scattering and ion imaging techniques to explore the partial oxidation of styrene. This experimental approach enhances the sensitivity to the extent that we can directly observe the partial oxidation product, styrene oxide, under UHV conditions. We note that partial oxidation exclusively occurs at high oxygen coverages, which we attribute to the reaction of styrene with electrophilic oxygen formed specifically at elevated coverages.

Introduction

Epoxides, with their chemical versatility, play a crucial role in the chemical industry. In 2022, ethylene oxide production reached 32 Mt, with an anticipated growth of approximately 50% from 2015 to 2030.[1] Due to the unique surface chemistry of alkene/silver systems, Ag-based catalysts have become the industrial standard for large-scale epoxidation.[2] Consequently, optimizing the production process can yield significant economic and environmental benefits, driving extensive research efforts under well-controlled ultra-high vacuum (UHV) conditions in the past to comprehensively understand the surface reaction pathway.[3–11] Investigating partial ethylene oxidation under UHV faces mainly two experimental challenges. First, the ethylene desorption rate is significantly faster than the partial oxidation reaction rate, leading to premature ethylene desorption. Second, the low reaction probability of molecular oxygen on silver complicates surface oxidation. These challenges are addressed through specific approaches such as the use of well-established substitutional oxidants under UHV conditions, including NO_2,[12] atomic oxygen (AO),[13,14] and ozone.[15] Additionally, derivatives of epoxides with stronger surface binding, such as norbornene,[16] styrene,[10,16–19] and 3,3-dimethyl-1-butene[20] are employed in corresponding experiments targeting for a detailed mechanistic understanding. UHV studies using these approaches have revealed that epoxide formation occurs via the intermediate formation of an oxametallacycle on the surface.[7,8,18,19,21–25] This intermediate exhibits an –O–C–C– structure connected at both ends to the metal surface, creating a five-membered ring with the silver surface. However, while the formation of the oxametallacycle is well-established through experimental studies and theoretical modeling, the role of surface oxygen remains unclear. Successful models describe the high selectivity in the olefine epoxidation by distinguishing between nucleophilic (O_{nuc}) and electrophilic oxygen (O_{elec}) atom species available at the surface.[26–28] Unlike O_{nuc}, which is primarily active in combustion, O_{elec} is believed to be the key species responsible for selective oxametallacycle and subsequent epoxide formation. In experiments achieving controlled O_{elec} production proves challenging due to the complex surface chemistry of oxidized silver surfaces. The identification of electrophilic oxygen typically relies on a distinctive shift observed in X-ray photoelectron spectroscopy (XPS).[29]

In recent UHV studies combining different surface science techniques, the structure of silver surfaces bearing O_{elec} was investigated employing XPS, scanning-tunnelling microscopy (STM), low-energy electron microscopy (LEEM), and photoemission electron microscopy (PEEM).[30,31] Oxidized silver surfaces were generated by exposing the surface to NO_2 as oxidizing agent. At low exposures, this process led to the well-known $p(4 \times 4)$-O surface reconstruction, marked by a characteristic nucleophilic oxygen signature in XPS. Distinctive XPS characteristics of electrophilic oxygen only become evident at high exposure levels, persisting on the surface even after thermally desorbing the nucleophilic oxygen. This active form of oxygen for epoxidation consistently coexists with subsurface oxygen (O_{sub}) as shown by distinct XPS peaks. The surface phase of active oxygen initially emerges at step edges and step bunches. Repeated cycles of NO_2 exposure, resulting in the formation of

[a] R. E. A. Dissanayake, A. C. Dorst, K. Benfreha, T. Schäfer
Institute of Physical Chemistry, University of Göttingen, Göttingen, Germany
E-mail: tschaef4@gwdg.de

[b] R. E. A. Dissanayake, A. C. Dorst, K. Benfreha, T. Schäfer
Max-Planck Institute for Multidisciplinary Sciences, Göttingen, Germany

[c] D. R. Killelea
Department of Chemistry and Biochemistry, Loyola University Chicago, Chicago, IL, United States

the $p(4 \times 4)$-O surface reconstruction followed by thermal desorption, lead to an increased concentration of the active phase.

In this study, we investigate the epoxidation of styrene on an oxidized Ag(111) surface under well-controlled UHV conditions, employing molecular beam surface scattering coupled with ion imaging detection. We create an active phase of oxidized silver using NO_2 following the procedures outlined by the authors of the study described above.[30,31] These prepared surfaces are then exposed to pulsed molecular beams of styrene, and we monitor the production of reaction products as a function of surface coverage. Our findings reveal the formation of styrene oxide at high coverages, coinciding with the presence of O_{elec}. However, when O_{elec} is depleted, no further partial oxidation occurs.

Results and Discussion

For our study, we employ two distinct methods to create oxidized Ag(111) surfaces, depending on the targeted surface structure. In Method 1, we generate O/Ag(111) with nucleophilic oxygen, characterized by the well-known $p(4 \times 4)$-O surface reconstruction. This involves Ar-ion sputtering of the surface for 20 min followed by annealing at 700 K under UHV conditions. Subsequently, the surface is exposed to a pulsed molecular beam comprising 10% NO_2 in He. Maintaining the surface temperature at 510 K enables the dissociation of NO_2 at the surface, yielding NO and atomic oxygen. At this temperature, NO desorbs, and nucleophilic oxygen remains at the surface.

Alternatively, in Method 2 we create an oxidized Ag(111) surface enriched with oxygen O_{elec} following the methods outlined by Böcklein *et al.* In combined studies of XPS and STM they identified and mapped the morphological features associated with active surface oxygen O_{elec} generated after NO_2 oxidation.[30,31] When exposed to intensive doses of NO_2, the morphology of the Ag(111) surface changes significantly. The characteristic step-and-terrace structure observed on uncovered, densely packed metal surfaces shifts to a surface with straight steps aligned along the [11-2] axis. It forms a striped phase with sharp LEED diffraction patterns of a $(7 \times \sqrt{3})$ superstructure visible in LEEM. The area covered by this phase scales with the peak intensity of the active electrophillic surface oxygen in the XPS, signifying a clear connection between this surface and O_{elec}.

The authors found that repetitive surface annealing above the desorption temperature of O_2, coupled with cooling and additional dosing without sputtering, resulted in the accumulation of this specific surface phase. This was evident from the amplified growth of the O_{elec} XPS peak throughout the desorption and adsorption cycles. Notably, the spectral features in the XPS spectra indicate that the near-surface region of the Ag crystal accumulates subsurface oxygen when oxidized by this procedure. This suggests that active oxygen O_{elec} is consistently accompanied by subsurface oxygen.

We achieve precise control over surface oxidation by analyzing temperature-programmed desorption (TPD) spectra of molecular oxygen following well-defined NO_2 molecular beam exposure times. The calculation of exposure is based on UHV pressure rise and molecular beam settings and is explained in detail in the Experimental Section. Figure 1 panel a) shows TPD curves for O/Ag(111) following Method 1 for surface oxidation, resulting in the formation of O_{nuc}.

The nature of NO_2 sticking is revealed by the TPD curves. It is evident that the oxygen desorption, and thus oxygen coverage, reaches saturation after an exposure of ca. 250 ML NO_2, which corresponds to an oxygen coverage of 0.375 ML.[32] The inset shows the O coverage as a function of NO_2 exposure, and from from the slope, the sticking probability (S) of NO_2 can be determined. The initial, or low-coverage, sticking probability, S_0, is the slope of the line near the origin, and we find that $S_0 =$ 0.0023. Figure 1 panel b) shows a plot of $S(\theta)$ vs θ_O, and shows that only a single adsorption site is required for NO_2 dissociation. This suggests that NO_2 dissociation is late and the NO fragment promptly desorbs to the gas phase as O adsorbs to

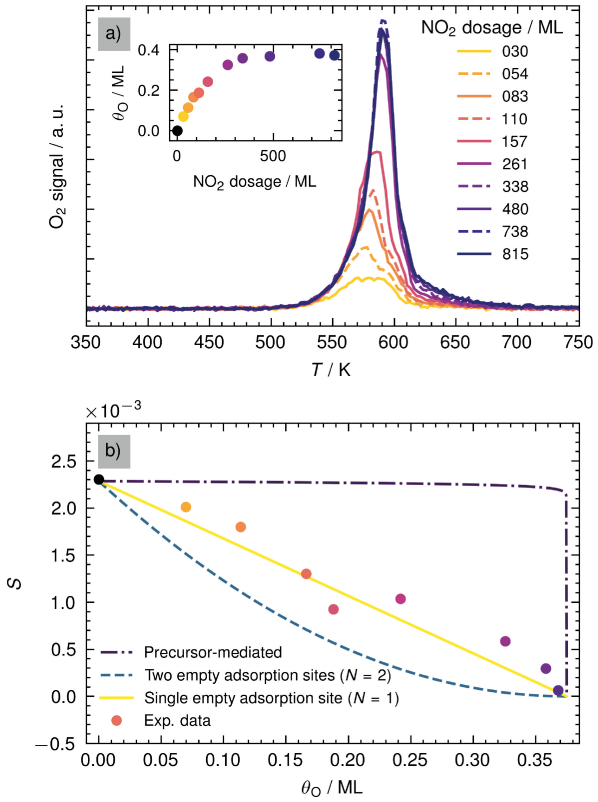

Figure 1. Panel a): Temperature programmed desorption spectra of molecular oxygen desorbing from Ag(111) for different exposures in monolayer equivalents (ML) to a pulsed molecular beam of 10% NO_2 in He. The calculation of exposure is based on UHV pressure rise and molecular beam settings and is explained in detail in the Experimental Section. The inset shows the dependence of oxygen atom coverage (θ_O) as function of exposure. We define the maximum coverage to be 0.375 ML as internal standard.[32] Panel b): Sticking probabilty S as function of surface coverage. We deduce the curve from the inset of panel a). The sticking probability depends linearly on the coverage indicating a direct dissociation mechanism necessitating only one empty adsorption site. We also draw expected curves for a precursor-mediated mechanism and for direct dissociation with one and two empty adsorption sites ($S(\theta) = S_0 \times (1 - \frac{\theta}{\theta_{max}})^N$) to guide the eyes.

the silver surface. We do not discern any significant variations when adjusting the translational energies in the incident molecular beam between 0.78 eV and 1.25 eV. Within the experiment's margin of uncertainty, also the reaction probability remains consistent for various molar fractions (10%, 5% and 2%) of $NO_2 + N_2O_4$ in He.

With oxidation procedure Method 1, we only observed O_{nuc} in the TPD spectra. However, for efficient partial styrene oxidation in molecular beam surface scattering experiments, we had to use Method 2 as oxidation procedure, which produces a Ag(111) surface with enriched O_{elec}. For such experiments, we employ several NO_2 desorption adsorption cycles (>5) for the oxidized silver surface as Böcklein *et al.*, creating O_{elec} in addition to the typical $p(4\times4)$-O surface reconstruction associated with O_{nuc}. In each cycle, we heat to 700 K without sputtering and achieve maximum oxygen coverage on the Ag(111) surface by exposing it for a duration of 3 min with the pulsed molecular beam of 10% NO_2 in He at 200 Hz.

We confirm the formation of subsurface oxygen by the TPD spectra presented in Figure 2 which exhibit clear indication for subsurface oxygen formation. Figure 2 panel a) displays TPD spectra for the two distinct preparation schemes. The dashed line represents the spectrum obtained after 20 min of surface sputtering followed by annealing at 700 K (Method 1). This method aligns with the preparation scheme employed for the spectra in and corresponds to the TPD of a $p(4\times4)$-O reconstructed surface. The solid line is the obtained TPD spectra after preparing the surface without sputtering after five cycles of desorption and adsorption following the method outlined by Böcklein *et al.* (Method 2). It corresponds to a surface with enriched activated oxygen O_{elec}. We notice the emergence of a shoulder within the desorption peak around 560 K. Previously, this shoulder has been unambiguously assigned to subsurface oxygen through experiments involving an atomic oxygen source for oxidizing the Ag(111) surface.[14,32] Figure 2 panel b) shows the corresponding TPD spectrum of Ag(111) after atomic oxygen exposure at 490 K. The shoulder in the spectrum is assigned to the desorption subsurface oxygen. For more information, see Refs. [14, 32]. In our experiments, we determine the additional oxygen uptake to be 25% by calculating the integrals of the temperature-programmed desorption TPD curves in Figure 2 panel a).

A strength of our approach is the ability to independently control the intensity of the two oxygen reagents at the surface. With the surface enriched with O_{elec} we direct styrene to the oxidized surface using a second molecular beam comprising 1% styrene in He and employ sliced ion imaging techniques to detect ions with the mass of styrene oxide after surface reaction.[33] We ionize desorbing products after each molecular beam pulse with a repetition rate of 10 Hz. Importantly, in these titration experiments we automatically deplete the surface's oxygen coverage by not introducing any additional oxygen; the NO_2 source stays turned off. As a result, the recorded signal of the styrene oxide reaction product reflects the reactivity on a surface with progressively diminishing oxygen coverage. Figure 3 shows the ionization region of desorbing reaction products and the styrene oxide signal as function of the

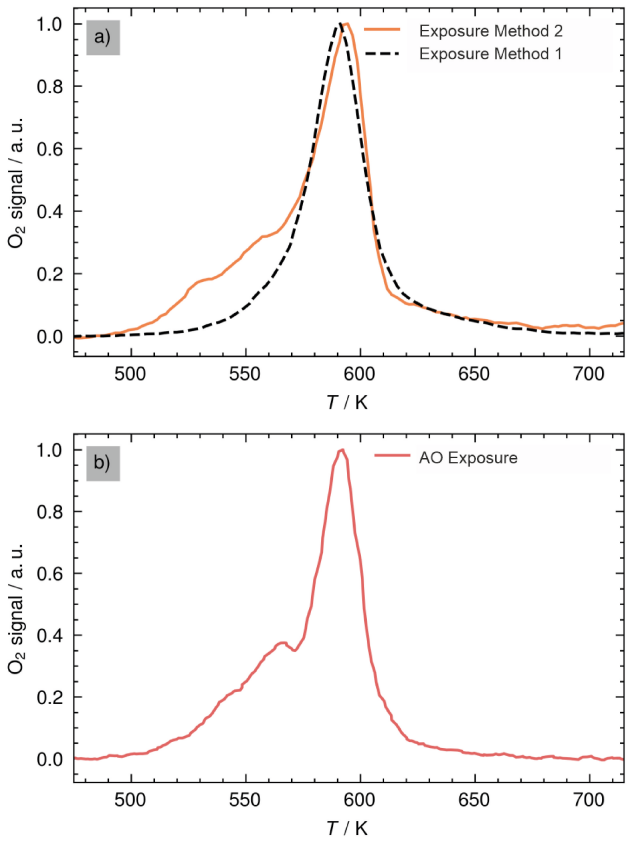

Figure 2. Panel a): Temperature programmed desorption spectra of recombinatively-desorbing O_2 from Ag(111). The dashed line depicts the spectrum acquired after 20 min of surface sputtering and subsequent annealing at 700 K. This approach mirrors the preparation method used for the spectra in Figure 1 and represents the TPD of a $p(4\times4)$-O reconstructed surface (Method 1). The solid line represents the TPD spectrum obtained after surface preparation without sputtering, following five cycles of desorption and adsorption as outlined by Böcklein *et al.* It corresponds to a surface with enriched activated oxygen O_{elec} (Method 2). We determine the additional oxygen uptake to be 25% by calculating the integrals of the temperature-programmed desorption TPD curves. Panel b): TPD spectrum after atomic oxygen (AO) dosage at 490 K from Ref. [14]. Subsurface oxygen emergence and desorption yields the shoulder peak around 560 K.

number of molecular beam pulses. Remarkably, after approximately 200 shots, the signal disappears, primarily due to the exhaustion of O_{elec} oxygen species critical for the epoxidation process on the surface.

We perform ionization of styrene oxide using a 264.75 nm laser output generated by a nanosecond Nd:YAG laser-pumped dye laser with an energy of 1 mJ. Subsequently, we detect styrene oxide products with a mass of 120 amu by temporally gating the micro-channel plates (MCPs) within the ion imaging detector to match the time-of-flight (ToF). Based on findings from previous experiments, we know that nanosecond laser ionization selectively generates ions exclusively from styrene oxide, effectively excluding ionization of mass isomers.[34]

In a second set of experiments, we determine the epoxidation probability as function of surface oxygen coverage. For this, we again prepare a fully oxygen-covered Ag(111) surface with O_{elec} by exposing it for 3 min with the pulsed

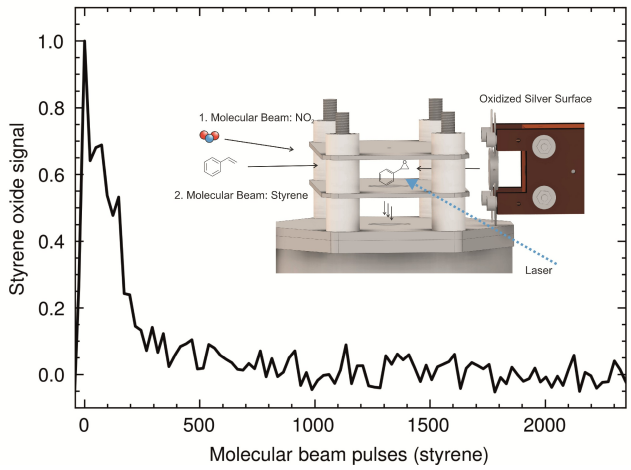

Figure 3. Integrated signal of styrene oxide as function of molecular beam pulses. The signal diminishes as a result of the consumption of reactive O_{elec} oxygen species. Inset: Experimental setup of the ionization region. We use the first molecular beam for controlled surface oxidation under UHV conditions with NO_2. The second molecular beam is used to introduce styrene pulses at a repetition rate of 10 Hz. We monitor the reaction products, specifically styrene oxide, at the same 10 Hz rate by ionizing them with 268 nm photons generated through a Nd:YAG laser-pumped dye laser. These ions are then directed into the time-of-flight (ToF) tube of an ion imaging detector which offers measurements of both mass and velocity.

molecular beam of 10% NO_2 in He at 200 Hz. Afterwards, we let the styrene molecular beam run for a specific time period, titrating the oxygen at the surface. After each time period we stop the molecular beam and measure the oxygen coverage by TPD. Figure 4 shows the integrated oxygen signal as function of styrene exposure. We calibrate the oxygen coverage to the values obtained from the TPD measurements shown in Figure 2 and indicate a complete monolayer coverage of 0.375 ML as dashed lines.

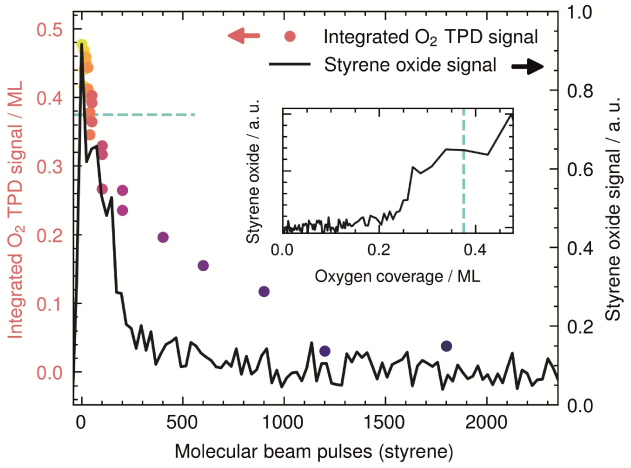

Figure 4. Colored points: Surface oxygen coverage after various styrene exposures. The coverage is determined from TPD spectra. Solid line: Styrene oxide signal when exposing the same oxidized surface to molecular beam pulses of styrene. We calibrate the oxygen coverage to the values obtained from the TPD measurements shown in and indicate a complete monolayer coverage of 0.375 ML as dashed lines. We extract the styrene oxide production as function of the surface oxygen coverage, which is shown in the inset.

In general, surface oxygen is depleted due to reaction with incoming styrene. However, partial oxidation of styrene to styrene oxide occurs exclusively at high surface oxygen coverage when O_{elec} is present indicated by coverage >0.375 ML. As soon as styrene has consumed O_{elec}, no partial oxidation is observed, despite ongoing consumption of surface oxygen. At low coverages, the interaction of styrene with surface oxygen must therefore yield different reaction products. We assume that combustion to CO_2 and water occurs. However, our experimental setup is unable to detect these masses effectively, primarily due to the intense ion signal at the corresponding ToF caused by photofragmentation of both, reactants and products. The inset of Figure 4 shows the detection of styrene oxide product as function of oxygen surface coverage. It clearly shows that partial oxidation occurs exclusively at high oxygen coverage. Again, the dashed line indicates a complete $p(4\times4)$-O monolayer of 0.375 ML.

In this context, we interpret our results as follows. When we prepare the oxidized surface through a sequence of desorption and adsorption cycles of NO_2, we generate both the typical $p(4\times4)$-O surface reconstruction and also domains of the active striped O_{elec} phase with the $\left(7\times\sqrt{3}\right)$ superstructure and subsurface oxygen, as observed by Böcklein *et al.*[31] When styrene subsequently interacts with this highly covered surface, it reacts with O_{elec}, resulting in the formation of styrene oxide. Once this reservoir is exhausted, the reaction with the nucleophilic $p(4\times4)$-O surface commences, leading to the complete combustion of styrene. The concurrent formation of O_{elec} and subsurface oxygen suggests that subsurface oxygen might indirectly alter the potential energy surface of the reaction pathways. As long as subsurface oxygen is available, this alteration could favor the formation of epoxides over the competitive pathway of complete combustion, for instance by influencing reaction barriers.

Conclusions

In conclusion, we have demonstrated the epoxidation of olefins on oxidized Ag(111) using molecular beam surface scattering in conjunction with ion imaging techniques. The heightened sensitivity of this method allowed us, for the first time, to detect reaction products in ultra-high vacuum conditions. These findings directly confirm that the partial oxidation of styrene occurs with the active, electrophilic form of surface oxygen, which we identify in TPD experiments. This form was previously experimentally determined as a striped O_{elec} phase with a $(7\times\sqrt{3})$ superstructure, coupled with subsurface oxygen.

Experimental

All the experiments were performed in a home-built molecular beam surface reaction chamber as described in Westphal *et al.* in detail.[34] We maintained a base pressure of $<2\times10^{-10}$ mbar by differentially pumping the chamber. The reactants, styrene (Carl Roth, 99.5%) and 10% NO_2 (AirLiquide, 99.5%) were seeded in He (AlphaGaz, >99.999%) and dosed onto the surface using a custom-

built pulsed solenoid nozzle (pulse width <80 μs).[35] The heatable nozzle provides a reservoir for liquids, so that the preparation of molecular beams containing room temperature liquids becomes possible.

The Ag(111) crystal (MaTecK, 99.99%) was mounted on a sample holder equipped with a Ta filament for resistive heating. Cooling was achieved using liquid nitrogen, enabling a broad temperature range from 100 K to 1200 K. Temperature measurements were conducted using a K-type thermocouple. The surface was cleaned via Ar^+ sputtering (2.00 kV, 2×10^{-7} mbar Ar) using a commercial ion gun (Staib Instruments IG-5-C), followed by annealing at 700 K for 30 min. We used a home-written LabVIEW™ program to change experimental parameters and data acquisition.

Desorbing products were ionized using focused laser radiation. Styrene oxide was ionized with nanosecond laser pulses of 264.75 nm and a repetition rate of 10 Hz using a Nd:YAG laser (Spectra-Physics, Quanta-Ray)-pumped dye laser (Sirah, Cobra-Stretch). NO_2 in the incoming molecular beam and desorbing O_2 in TPD experiments were ionized using a regeneratively amplified femtosecond laser (Spectra-Physics, Solstice Ace). The laser generates laser pulses of 800 nm with 35 fs at a repetition rate of 1 kHz.

Ionized molecules were accelerated in a ToF tube to reach the ion imaging detector using an ion lens design inspired by the work of Eppink and Parker[36] and described in more detail here.[37,38] The ion lens setup allows for velocity map imaging of surface desorbing products using micro-channel plates (Topag, MCP 56-15) coupled to a phosphor screen (Proxivision P43). The illuminations of the phosphor screen were recorded using a CMOS camera (Basler aceacA 1920 – 155 μm, 1920×1200 px). To detect specific masses based on their ToF, we gated the high voltage supply of the MCP.

TPD spectra were recorded using the femtosecond laser output as ionization source and detecting O_2 at the imaging detector with a linear heating rate of 4 K/s^{-1}.

For dosing experiments, we calculate the NO_2 exposure in monolayer equivalents as follows. By using the pumping speed of the surface chamber and observing the pressure rise in the surface chamber when the molecular beam is turned on, we determine the number of molecules entering the surface chamber per molecular beam pulse. For this, we first calibrate the ion gauge in the surface chamber to the sensitivity of the NO_2/He mixture using a residual gas analyzer (RGA) attached to the chamber. We additionally consider the equilibrium between NO_2 and N_2O_4 using the equilibrium constant K_p of 0.147 at room temperature, thereby calculating the total amount of NO_2 as the reaction partner. We account for the focusing of heavier masses in the molecular beam center by conducting measurements using mixtures of Ar and He for comparison. Considering these parameters, we determine the number of NO_2 molecules in a molecular beam pulse to be 4.0×10^{11}. Taking into account the number of silver atoms per area of 1.38×10^{19} m^{-2},[39] and a molecular beam diameter of 3 mm^2, we calculate 0.01 ML $pulse^{-1}$.

Acknowledgements

R.E.A.D. acknowledges funding from the Humboldt Foundation through a Georg Forster research fellowship. A.C.D. acknowledges support from ICASEC at the University of Göttingen. T.S. acknowledges funding from the Deutsche Forschungsgemeinschaft under grants SCHA 1946/5-1 and INST 186/1302-1, as well as support from the Deutscher Akademische Austauschdienst (DAAD) (Grant 57651434). D.R.K. acknowledges support from the National Science Foundation under award CHE-2155068 and from ICASEC at the University of Göttingen. We acknowledge Sharani Roy for stimulating discussion. Open Access funding enabled and organized by Projekt DEAL.

Conflict of Interests

The authors declare that the research was conducted in the absence of any commercial or financial relationships that could be construed as a potential conflict of interest.

Data Availability Statement

The data that support the findings of this study are available from the corresponding author upon reasonable request.

Keywords: molecular beam · surface scattering · styrene epoxidation · Ag(111) · ion imaging

[1] A. R. (ChemIntel360), Market Volume of Ethylene Oxide Worldwide from 2015 to 2022, with a Forecast for 2023 to 2030 (in Million Metric Tons), Can Be Found under https://www.statista.com/statistics/1245260/ethylene-Oxide-Market-Volume-Worldwide/ **2023**.
[2] H. Li, A. Cao, J. K. Nørskov, *ACS Catal.* **2021**, *11*, 12052.
[3] C. Campbell, *J. Catal.* **1986**, *99*, 28.
[4] R. A. Van Santen, H. P. C. E. Kuipers, *The Mechanism of Ethylene Epoxidation*, pages 265–321, Advances in Catalysis, Elsevier **1987**.
[5] S. Tan, *J. Catal.* **1987**, *106*, 54.
[6] G. S. Jones, M. Mavrikakis, M. A. Barteau, J. M. Vohs, *J. Am. Chem. Soc.* **1998**, *120*, 3196.
[7] S. Linic, M. A. Barteau, *J. Am. Chem. Soc.* **2001**, *124*, 310.
[8] S. Linic, M. A. Barteau, *J. Am. Chem. Soc.* **2003**, *125*, 4034.
[9] M.-L. Bocquet, A. Michaelides, D. Loffreda, P. Sautet, A. Alavi, D. A. King, *J. Am. Chem. Soc.* **2003**, *125*, 5620.
[10] F. J. Williams, D. P. C. Bird, A. Palermo, A. K. Santra, R. M. Lambert, *J. Am. Chem. Soc.* **2004**, *126*, 8509.
[11] T. E. Jones, T. C. R. Rocha, A. Knop-Gericke, C. Stampfl, R. Schlögl, S. Piccinin, *ACS Catal.* **2015**, *5*, 5846.
[12] S. R. Bare, K. Griffiths, W. N. Lennard, H. T. Tang, *Surf. Sci.* **1995**, *342*, 185.
[13] H. Umemoto, H. Kusanagi, *J. Phys. D* **2008**, *41*, 225505.
[14] J. Derouin, R. G. Farber, S. L. Heslop, D. R. Killelea, *Surf. Sci.* **2015**, *641*, L1.
[15] M. Karatok, M. G. Sensoy, E. I. Vovk, H. Ustunel, D. Toffoli, E. Ozensoy, *ACS Catal.* **2021**, *11*, 6200.
[16] J. T. Roberts, R. J. Madix, *J. Am. Chem. Soc.* **1988**, *110*, 8540.
[17] S. Hawker, C. Mukoid, J. P. S. Badyal, R. M. Lambert, *Surf. Sci.* **1989**, *219*, L615.
[18] A. Klust, R. J. Madix, *Surf. Sci.* **2006**, *600*, 5025.
[19] A. Klust, R. J. Madix, *J. Am. Chem. Soc.* **2006**, *128*, 1034.
[20] C. Mukoid, S. Hawker, J. P. S. Badyal, R. M. Lambert, *Catal. Lett.* **1990**, *4*, 57.
[21] S. Linic, M. A. Barteau, *J. Am. Chem. Soc.* **2001**, *124*, 310.
[22] M. A. Barteau, *Top. Catal.* **2003**, *22*, 3.
[23] J. W. Medlin, M. A. Barteau, J. M. Vohs, *J. Mol. Catal. A* **2000**, *163*, 129.
[24] J. W. Medlin, M. A. Barteau, *J. Phys. Chem. B* **2001**, *105*, 10054.
[25] L. Zhou, R. J. Madix, *J. Phys. Chem. C* **2008**, *112*, 4725.
[26] V. I. Bukhtiyarov, M. Hävecker, V. V. Kaichev, A. Knop-Gericke, R. W. Mayer, R. Schlögl, *Phys. Rev. B* **2003**, *67*, 235422.
[27] E. A. Carbonio, T. C. R. Rocha, A. Y. Klyushin, I. Píš, E. Magnano, S. Nappini, S. Piccinin, A. Knop-Gericke, R. Schlögl, T. E. Jones, *Chem. Sci.* **2018**, *9*, 990.
[28] A. Michaelides, K. Reuter, M. Scheffler, *J. Vac. Sci. Technol. A* **2005**, *23*, 1487.
[29] T. E. Jones, R. Wyrwich, S. Böcklein, E. A. Carbonio, M. T. Greiner, A. Y. Klyushin, W. Moritz, A. Locatelli, T. O. Menteş, M. A. Niño, A. Knop-

Gericke, R. Schlögl, S. Günther, J. Wintterlin, S. Piccinin, *ACS Catal.* **2018**, *8*, 3844.
[30] S. Günther, S. Böcklein, J. Wintterlin, M. A. Niño, T. O. Menteş, A. Locatelli, *ChemCatChem* **2013**, *5*, 3342.
[31] S. Böcklein, S. Günther, J. Wintterlin, *Angew. Chem. Int. Ed.* **2013**, *52*, 5518.
[32] M. E. Turano, R. G. Farber, E. C. N. Oskorep, R. A. Rosenberg, D. R. Killelea, *J. Phys. Chem. C* **2019**, *124*, 1382.
[33] D. J. Harding, J. Neugebohren, H. Hahn, D. J. Auerbach, T. N. Kitsopoulos, A. M. Wodtke, *J. Chem. Phys.* **2017**, *147*.
[34] G. Westphal, M. Wallrabe, T. Schäfer, *J. Phys. Chem. C* **2019**, *124*, 799.
[35] G. B. Park, B. C. Krüger, S. Meyer, D. Schwarzer, T. Schäfer, *J. Chem. Phys.* **2016**, *144*, 194308.
[36] A. T. J. B. Eppink, D. H. Parker, *Rev. Sci. Instrum.* **1997**, *68*, 3477.
[37] A. C. Dorst, R. E. A. Dissanayake, D. Schauermann, S. Knies, A. M. Wodtke, D. R. Killelea, T. Schäfer, *Front. Chem.* **2023**, *11*.
[38] A. C. Dorst, F. Güthoff, D. Schauermann, A. M. Wodtke, D. R. Killelea, T. Schäfer, *Phys. Chem. Chem. Phys.* **2022**, *24*, 26421.
[39] A. Raukema, D. A. Butler, F. M. A. Box, A. W. Kleyn, *Surf. Sci.* **1996**, *347*, 151.

Manuscript received: April 10, 2024
Version of record online: ■■, ■■

RESEARCH ARTICLE

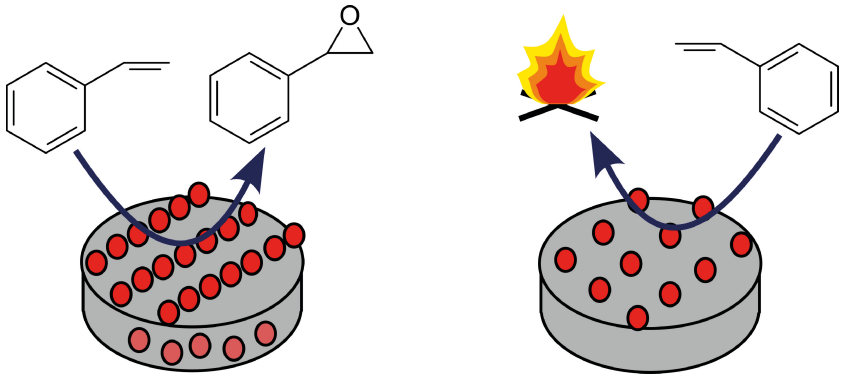

*R. E. A. Dissanayake, A. C. Dorst, K. Benfreha, D. R. Killelea, T. Schäfer**

The epoxidation of olefins on silver surfaces is an important industrial process on a large scale. This paper presents microscopic insights of styrene oxidation on Ag(111) under well-controlled ultra-high vacuum conditions. Epoxidation exclusively takes place at elevated oxygen coverages, coinciding with the emergence of electrophilic oxygen. Upon depletion of electrophilic oxygen, residual nucleophilic oxygen triggers complete combustion.

SPACE RESERVED FOR IMAGE AND LINK

Share your work on social media! *ChemCatChem* has added Twitter as a means to promote your article. Twitter is an online microblogging service that enables its users to send and read short messages and media, known as tweets. Please check the pre-written tweet in the galley proofs for accuracy. If you, your team, or institution have a Twitter account, please include its handle @username. Please use hashtags only for the most important keywords, such as #catalysis, #nanoparticles, or #proteindesign. The ToC picture and a link to your article will be added automatically, so the **tweet text must not exceed 250 characters**. This tweet will be posted on the journal's Twitter account (follow us @ChemCatChem) upon publication of your article in its final form. We recommend you to re-tweet it to alert more researchers about your publication, or to point it out to your institution's social media team.

ORCID (Open Researcher and Contributor ID)

Please check that the ORCID identifiers listed below are correct. We encourage all authors to provide an ORCID identifier for each coauthor. ORCID is a registry that provides researchers with a unique digital identifier. Some funding agencies recommend or even require the inclusion of ORCID IDs in all published articles, and authors should consult their funding agency guidelines for details. Registration is easy and free; for further information, see http://orcid.org/.

Rasika E. A. Dissanayake http://orcid.org/0000-0001-7535-6552
Arved C. Dorst http://orcid.org/0000-0001-5258-6953
Kerim Benfreha
Daniel R. Killelea http://orcid.org/0000-0001-6965-5644
Tim Schäfer http://orcid.org/0000-0001-9468-0470